Effect of Initial FeO Content and $CaO:SiO_2$ Ratio on the Reduction Smelting Kinetics of the $CaO\text{-}SiO_2\text{-}MgO_{satd.}$-FeO Slag System

JONG BAE KIM and IL SOHN

The effect of the initial FeO content and $CaO:SiO_2$ ratio (CaO mass pct/SiO_2 mass pct) on the reduction smelting of FeO with carbon flake addition is investigated in the $CaO\text{-}MgO_{satd.}\text{-}SiO_2$-FeO slag system at 1823 K (1550 °C). Carbon rapidly reacted with FeO in the molten slag, causing both foaming and compositional changes in the slag. As FeO is reduced, the MgO saturation is modified, and solid precipitants, including MgO and other complex oxides, were observed, which significantly affected the slag properties, including the viscosity and foaming behavior. The solid-phase fraction and viscosity were estimated from changes in the measured FeO content over time using the thermochemical software FactSage. The iron recovery, which is distinguished from the amount of reduced Fe droplets, showed opposite behavior to the measured maximum foaming height and modified foaming index. According to the FeO mass transfer coefficient considering slag foaming at various initial FeO contents and $CaO:SiO_2$ ratios, the reduction rate was optimal at higher initial FeO contents and a $CaO:SiO_2$ ratio of 2.0, which did not correspond to the optimal iron recovery at an initial FeO content of 44 mass pct and above and a $CaO:SiO_2$ ratio of 1.2. The results showed that slag foaming may increase the reduction kinetics, but the slag composition needs to be optimized for greater iron recovery.

https://doi.org/10.1007/s11663-017-1143-1

I. INTRODUCTION

SINCE the first commercial electric arc furnace (EAF) in 1907, EAFs have been widely used to meet recycling demands and produce steel with a lower carbon footprint. Newly designed furnaces allow scrap pre-heating systems, single-bucket operation, and supersonic lances for gas injection. These innovations have not only minimized energy consumption, but also provided solutions to environmental problems using recyclable raw materials such as scrap and other Fe-rich by-products.[1–4] However, attempts to utilize partially reduced iron-containing by-products with a total Fe content below 50 pct and significant gangue content required additional carbon addition for reduction, which induced significant compositional changes to FeO and MgO in the EAF slags during operation, subsequently disturbing optimal slag foaming and lowering the operational stability.

JONG BAE KIM and IL SOHN are with the Department of Materials Science and Engineering, Yonsei University, 262 Seongsanno, Seodaemun-gu, 120-749 Seoul, Korea. Contact e-mail: ilsohn@yonsei.ac.kr
Manuscript submitted December 1 2017.
Article published online November 28, 2017.

Several previous works have studied FeO reduction in slag and the subsequent foaming behavior. Ozawa *et al.*[5] described the carbothermic reduction of EAF slags containing a FeO content as high as 60 mass pct and concluded that reduction is controlled by the liquid-phase mass transfer of FeO to carbon and that a higher $CaO:SiO_2$ ratio (CaO mass pct/SiO_2 mass pct) increased the reduction rate due to increased slag foaming. Dankwah *et al.*[6] reduced FeO in EAF slags with coke and waste polymers, which showed significant CO generation, induced foaming, and promoted faster reduction kinetics within 6 minutes of the initial reduction. Qiu *et al.*[7] conducted a series of room-temperature experiments to identify the parameters that effect slag foaming during chemical reactions and found that a higher slag viscosity extended the foaming elimination time, but reduced the maximum foaming height. Higher surface tension was also found to suppress foaming, and the co-existence of solid particles in the solution significantly increased the viscosity. Busolic *et al.*[8] investigated the recovery of iron from copper flash smelting slags with coke, which indicated the possibility of reducing FeO in the slag, but did not distinguish between the reduced Fe droplet and subsequent iron recovery.

Heo *et al.*[9] discussed in detail the promotion of FeO reduction with carbon in similar $CaO\text{-}MgO\text{-}SiO_2$-

Al_2O_3-FeO copper smelting slags at FeO contents above 50 mass pct during slag foaming, but differentiated between iron recovery and FeO reduction and observed suppressed iron recovery due to excessive foaming.

Past literature on the reduction rate of FeO in slag by carbon identified slag foaming to accelerate reduction through the generation of CO gas from the C-FeO reaction, which strongly agitates the melt, increasing the liquid-phase mass transfer and subsequently the FeO reduction rate.[9,10] Generally, the reduction of FeO with carbon can be expressed according to the following Eqs. [1] through [3].[8]

$$(\text{FeO}) + \text{C} = \text{Fe(l)} + \text{CO(g)}\ \ \Delta\text{G}^\circ = 141,731.2 - 139.5 \times \text{T (J/mol)}, \quad [1]$$

$$(\text{FeO}) + \text{CO(g)} = \text{Fe(l)} + \text{CO}_2\text{(g)}\ \Delta\text{G}^\circ = -24,905.5 + 31.6 \times \text{T (J/mol)}, \quad [2]$$

$$\text{C(s)} + \text{CO}_2\text{(g)} = 2\text{CO(g)}\ \Delta\text{G}^\circ = 166,636.7 - 171.1 \times \text{T (J/mol)}, \quad [3]$$

where Eq. [1] is rate limiting, and through agitation of the melt by slag foaming, the overall kinetics are accelerated.[11–14] Other works have suggested that carbon is the dominant factor in determining the reduction rate and the reduction degree of FeO in the slag.[15,16] Thus, understanding slag foaming during the reduction of FeO with carbon and its effect on mass transfer is essential in controlling the reduction kinetics.

Ito and Fruehan[17,18] proposed a foaming index to describe the foaming stability of the slag, which corresponds to a greater tendency of a slag to foam. The foaming index was characteristic of the slag composition and physically correlated to the gas traveling time in the slag. The foaming index for a fully liquid slag can be expressed by the following Eq. [4].

$$\sum\nolimits_{\text{fully liquid}}(s) = \kappa \times \frac{\eta}{\sqrt{(\sigma \times \rho)}}, \quad [4]$$

where κ, ρ (kg/m^3), σ (mN/m), and η (N s/m^2) are the characteristic constant, density, surface tension, and dynamic viscosity of a foaming slag, respectively, at a specific temperature. Thus, a modified foaming index can be estimated using the following Eq. [5] by substituting the dynamic viscosity of the fully liquid slag.

$$\sum\nolimits_{\text{with particles}}(s) = \kappa \times \frac{\eta^o}{(1 - \alpha \times f)^n \times \sqrt{(\sigma \times \rho)}} \quad [5]$$

The slag density was obtained from previous works.[19,20] An empirical value of the characteristic constant, κ, is not available for the CaO-$MgO_{satd.}$-SiO_2-FeO system in the present study, but for other slag systems, this constant has been identified to broadly range from 115 to 999.[21] Considering the saturation condition of the present quaternary slag system, a value of 999 was used based on the work of Kim *et al.*[22] on the CaO-SiO_2-FeO-$MgO_{satd.}$-based quinary slag system.

However, the influence of temperature on the slag density was neglected since it generally shows a small dependence on temperature.[23,24] Morales *et al.*[25] also indicated that while foaming can improve mass transport and provide energy savings in an EAF, excessive foaming can disturb typical oxygen steelmaking operations due to slag overflow. However, studies regarding slag foaming for a broad and extensive range of FeO contents in the CaO-SiO_2-FeO-based EAF slag system are limited. In addition, slag foaming with MgO in the CaO-SiO_2-FeO-based slag is yet to be fully understood, even though typical EAF slags contain 10 mass pct or more MgO, which is near MgO saturation in the slag. Thus, as FeO reduction by carbon proceeds in the slag and iron is recovered in the iron reservoir, the near-saturated MgO in the slag becomes oversaturated due to the lower FeO content, resulting in solid precipitation within the melt.

According to past studies,[8,9,18] solid particles, such as Ca_2SiO_4 (olivine) or MgO (periclase) precipitants, co-existing in the liquid slag can affect foaming, while solid particles dispersed in the melt increase the viscosity.

Although several studies regarding slag foaming or FeO reduction have been conducted independently, detailed investigations of slag foaming during the reduction of a wide range of FeO contents by carbon in the CaO-SiO_2-$MgO_{satd.}$-FeO EAF slag system are limited. Furthermore, iron recovery after Fe droplet formation and its evaluation with respect to slag composition are not well understood.

In this study, the reduction smelting kinetics of FeO and iron recovery in the CaO-SiO_2-$MgO_{satd.}$-FeO slag system using carbon flakes at 1823 K (1550 °C) were investigated. The effect of slag foaming during reduction and the subsequent participation of solid particles co-existing in the slag on the iron recovery was identified. In particular, the effect of various initial FeO contents as high as 60 mass pct and CaO:SiO_2 ratios between 0.2 to 5.0 on the reduction kinetics was determined. The liquid-phase mass transfer coefficient of FeO, considering slag foaming, was also estimated to understand the kinetics after carbon addition.

II. EXPERIMENTAL METHODS AND PROCEDURES

A. *Sample Preparation*

The samples were prepared from reagent-grade FeO, MgO, SiO_2, and $CaCO_3$. $CaCO_3$ was calcined for 12 hours in a box furnace at 1273 K (1000 °C) to produce CaO, similar to past works. The slag compositions were chosen from the MgO-saturated compositions of past works, which varied depending on the CaO-SiO_2-FeO slag composition.[26,27] The slag compositions of the

Table I. Pre-experimental Weighed Composition of the CaO-$MgO_{satd.}$-SiO_2-FeO Slag System Used in the Present Work

Sample	Pre-experimental (Composition, Mass Pct)				
	CaO	MgO	SiO_2	FeO	CaO:SiO_2 (Mass Ratio)
F1	19.20	12.00	16.00	52.80	1.20
F2	21.60	12.00	18.00	48.40	1.20
F3	24.00	12.00	20.00	44.00	1.20
F4	28.80	12.00	24.00	35.20	1.20
F5	33.60	12.00	28.00	26.40	1.20
B1	25.00	10.00	5.00	60.00	5.00
B2	22.00	10.00	8.00	60.00	2.75
B3	21.00	10.00	9.00	60.00	2.33
B4	20.00	10.00	10.00	60.00	2.00
B5	16.36	10.00	13.64	60.00	1.20
B6	10	10.00	20.00	60.00	0.50
B7	5	10.00	25.00	60.00	0.20

No compositional changes were observed during pre-melting, as verified by XRF.

present work are provided in Table I. A fixed amount of MgO was added into the slag, and this undersaturation of MgO becomes saturated through dissolution of the MgO crucible. The samples were pre-melted in a box furnace for 5 hours at 1823 K (1550 °C) using a Pt-10Rh crucible (ϕ = 44 mm× H = 47 mm, 42 g) under a 1 slm flow of UHP-Ar (99.9999 vol. pct) gas similar to previously followed practices.[28,29] No compositional changes were observed after pre-melting, and the solidified slag samples were crushed using a ball mill (Pulverisette 0, FRITSCH, Germany) to approximately 4 mm pieces. Finally, 200 g of pulverized slag was used in the experiments.

B. *Reduction Smelting Procedure*

A high-frequency induction furnace (KP 1000, Eltek high-frequency induction furnace, Eltek, Anyang, Korea), depicted in Figure 1(a), was used. First, 100 g of electrolytic iron flakes (99.9 mass pct, TOHO ZINC, Gunma, Japan), which filled a depth of approximately 6 mm in a molten iron reservoir at 1823 K (1550 °C), was melted in a MgO crucible (99.9 mass pct, OD = 60 mm, ID = 50 mm, H = 120 mm, Toda, Tokyo, Japan). The quartz tube that enclosed the crucible and reacting materials was initially evacuated with a rotary pump and filled with 1 slm UHP-Ar (99.9999 vol. pct) to prevent the samples from oxidizing during heating. All gases were purified through glass columns of $CaSO_4$ and soda lime to eliminate moisture and CO_2. A graphite holder (99.999 mass pct, OD = 70 mm, ID = 64 mm, H = 130 mm, Woojin Carbon, Seoul, Korea) was used as a susceptor. A porous insulation brick composed of mainly MgO was placed between the quartz tube and the graphite susceptor to minimize heat loss.

A target temperature of 1823 K (1550 °C) was calibrated with a reference B-type thermocouple within ± 2 K. A fixed heating rate of 12.9 K/min was used until reaching 773 K (500 °C), then 17.5 K/min was used until reaching 1823 K (1550 °C). After reaching the target temperature, a holding time of 1 hour was applied to fully melt the electrolytic iron. Then, the slag was inserted into the MgO crucible containing the molten iron using a quartz tube (OD = 20 mm, ID = 18 mm, H = 600 mm) and held for an additional 1 hour to completely melt the slag and obtain MgO saturation. After visual verification of the fully molten iron and slag, FeO in the slag was reduced for a maximum of 1 hour using solid carbon flakes in a ratio of 1.2 moles per mol FeO. The carbon flakes were rectangular parallelepipeds and had an average volume of 5.23 mm^3 (SD ± 0.12), an average length of 0.91 mm (SD ±0.34), and a fixed thickness of 1 mm. These simplified dimensions were used to estimate the reaction surface area of the carbon for kinetic analysis. Ar gas flow was suspended once carbon was added into the melt, and the subsequent atmosphere was maintained from the generation of CO and CO_2 gas when FeO was reduced by carbon.

A quartz sampling tube (OD = 4 mm, ID = 2 mm, H = 600 mm) was used to obtain approximately 2 g samples of slag 5, 10, 30, and 60 minutes after the carbon flakes were added into the MgO crucible. The slag composition was determined using ICP-OES (induction coupled plasma-optical emission spectroscopy, Agilent OES-750, Santa Clara, California). The wet analysis of Fe^{2+} based on the JIS M 8212 and KS E ISO 5416 : 2011 standard was used for the analysis of metallic Fe, and the KS E ISO 2597-1 : 2007 standard was used to determine the total Fe content in the slag.

The modified foaming index, the details of which will be provided later, and the tendency of the slag to foam can be qualitatively correlated to the measured maximum foaming height represented by the slag solidified on the MgO crucible wall. Slags having a high modified foaming index results in a higher maximum foaming height. In the present work, the majority of the reduction occurred within 10 minutes after carbon addition, and the maximum foaming height was also typically observed after 10 minutes. The maximum foaming height measured as a function of time is provided in Figure 1(b) and the different slag compositions had similar maximum foaming heights. The final content of carbon in the iron reservoir was dependent on the slag composition, with a maximum average content of approximately 0.06 mass pct.

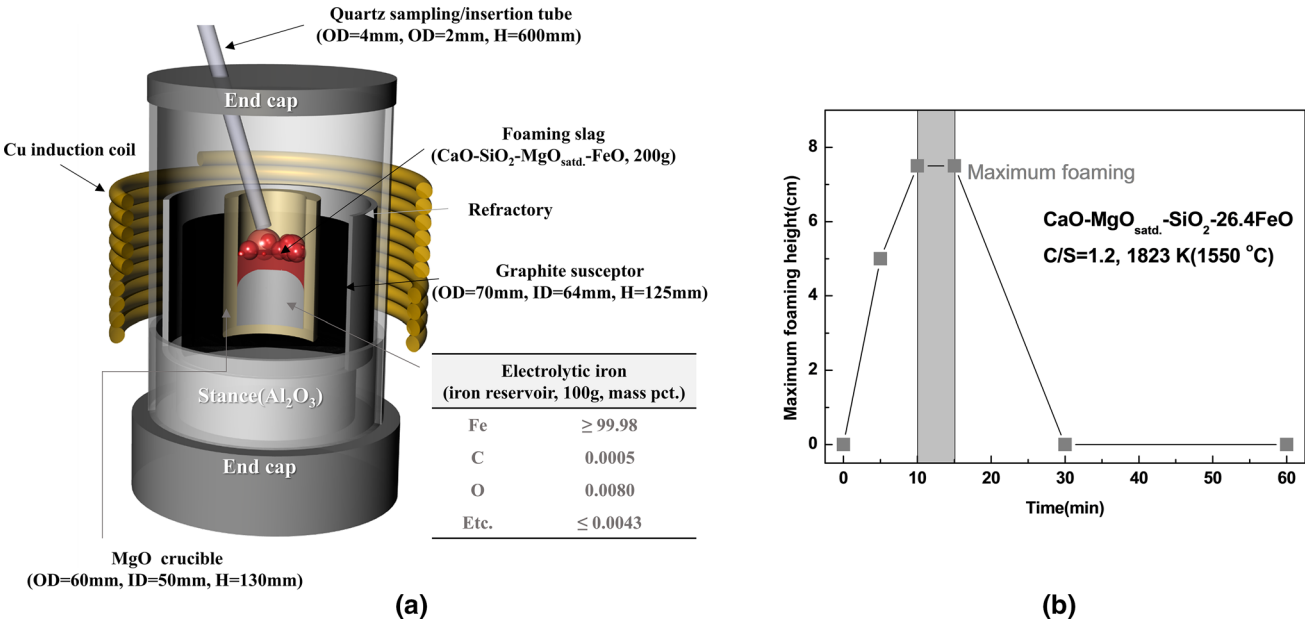

Fig. 1—(*a*) Schematic diagram of the induction furnace for smelting reduction and subsequent foaming at 1823 K (1550 °C) and (*b*) typical maximum foaming height measured as a function of time.

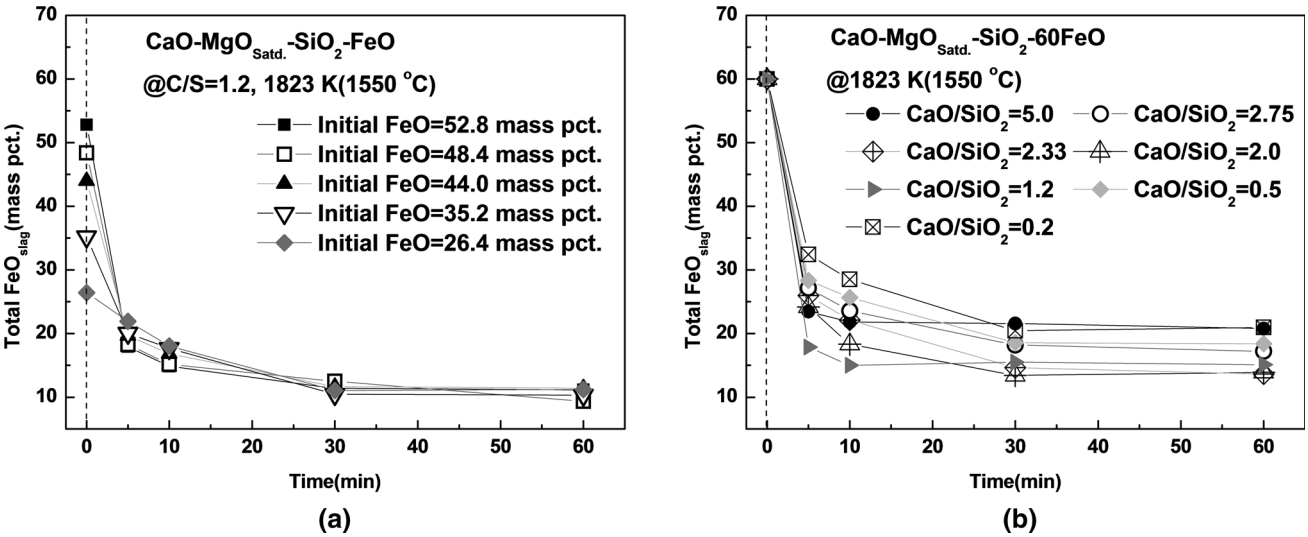

Fig. 2—Effect of varying (*a*) initial FeO content at fixed $CaO:SiO_2$ ratio of 1.2 and (*b*) $CaO:SiO_2$ ratio at FeO of 60 mass pct on the total FeO content during reduction with carbon flakes in $CaO-MgO_{satd.}-SiO_2-FeO$ at 1823 K (1550 °C).

All experiments were conducted at least 3 times to ensure reproducibility. The first test was done to collect slag samples at defined intervals to identify compositional changes over time. Other redundant tests were done for 60 minutes without sampling to determine the final reduction ratio of FeO more precisely.

III. RESULTS AND DISCUSSION

A. *Effect of Slag Composition and Foaming on Iron Recovery*

Figures 2(a) and (b) show the variation in the total FeO in the slag after carbon flake addition as a function of reduction time for various initial FeO contents and $CaO:SiO_2$ ratios, respectively. The final FeO content after 60 minutes decreases to approximately 10 to 15 mass pct in the $CaO-MgO_{satd.}-SiO_2-FeO$ slag systems with various initial FeO contents at a fixed $CaO:SiO_2$ ratio of 1.2. The final FeO content after 60 minutes is comparatively higher in the systems with various $CaO:SiO_2$ ratios at an initial 60 mass pct FeO. The results indicate that the bulk of the FeO reduction occurs within 10 minutes, due to the high reaction surface area of the carbon flakes. As a result, the change in slag composition, reduced Fe droplet formation, foaming, and solid particle precipitation due to the oversaturation of MgO in the slag as FeO is reduced would likely be pronounced during reduction.

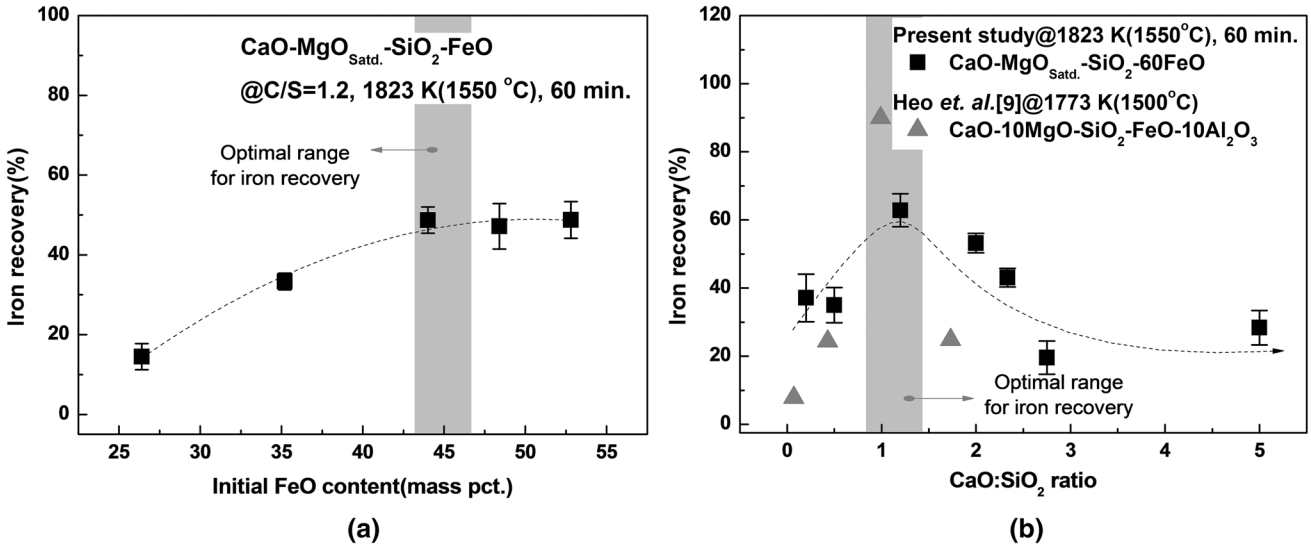

Fig. 3—Effect of varying (*a*) initial FeO content at fixed CaO:SiO$_2$ ratio of 1.2 and (*b*) CaO:SiO$_2$ ratio at FeO of 60 mass pct after carbon flake additions on iron recovery in CaO-MgO$_{satd.}$-SiO$_2$-FeO at 1823 K (1550 °C) for 60 min.

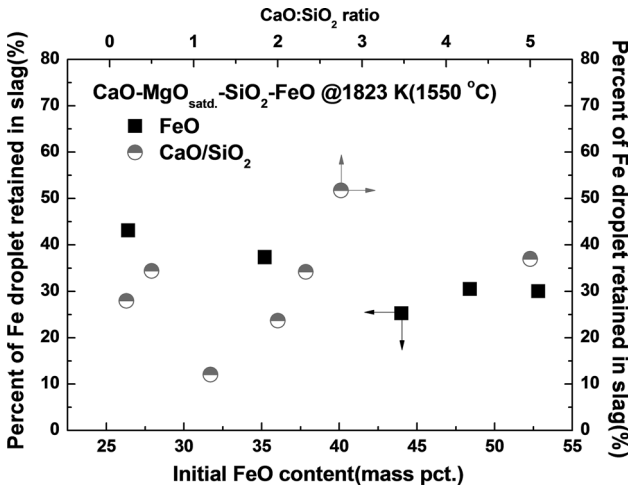

Fig. 4—Percent of reduced Fe droplet suspended within the foaming slag plotted as a function of initial FeO content and CaO:SiO$_2$ ratio in CaO-MgO$_{satd.}$-SiO$_2$-FeO at 1823 K (1550 °C).

Figures 3(a) and (b) show the effect of various initial FeO contents at a fixed CaO:SiO$_2$ ratio of 1.2 and various CaO:SiO$_2$ ratios at an initial FeO of 60 mass pct, respectively, on iron recovery 60 minutes after carbon flake addition. As carbon reacts with FeO in the slag, reduced Fe droplets form, and the slag composition changes over time. The amount of reduced Fe droplets collected in the initial 100 g molten iron reservoir corresponds to the iron recovery. According to Heo *et al.*,[9] the amount of Fe droplets collected in the iron reservoir can be maximized with the appropriate CaO:SiO$_2$ ratio, and the iron recovery can be expressed by the following Eq. [6].

$$\text{Iron recovery (mass pct)} = \left(\frac{\text{mass increment of Fe}_{\text{iron reservoir}}(g)}{\text{mass of Fe}_{\text{initial slag}}(g)}\right) \times 100 \quad [6]$$

Iron recovery should be distinguished from the amount of reduced FeO and resulting Fe droplets, since some of the reduced Fe metal droplets are suspended in the slag due to foaming. Although slag foaming enhances the liquid-phase mass transfer coefficient of FeO in the molten slag and increases the reduction kinetics,[10,30] the reduced Fe droplets must coalesce and pass through the foamy slag layer for collection in the molten iron reservoir to achieve a greater Fe yield. Thus, iron recovery behaves opposite to the foaming behavior due to the resistance caused by excessive gas evolution, which inhibits the reduced Fe droplets from coalescing and descending through the foamy slag. Furthermore, as FeO is reduced, the MgO saturation point for the reduced FeO content becomes oversaturated and MgO precipitation occurs. The presence of precipitation in the slag melt increases the viscosity and affects the foaming characteristics.

In Figure 3(a), the iron recovery after 60 minutes of reduction increases with the initial FeO content up to 44 mass pct and plateaus after 44 mass pct. A higher initial FeO content in the slag and subsequent reduction results in greater foaming and increased mass transfer, which increases the iron recovery. Greater iron recovery beyond the optimal iron recovery of 44 mass pct and above, even with an exceptionally high FeO content and smaller slag liquid volume, is not possible due to the greater fraction of solid particles formed within the slag, which affects the apparent viscosity, as will be discussed in subsequent sections. Figure 3(b) shows the iron recovery as a function of the CaO:SiO$_2$ ratio. At higher CaO:SiO$_2$ ratios, the iron recovery shows a concave upward parabolic trend with a maximum at 1.2 and subsequently decreases at higher CaO:SiO$_2$ ratios. Iron recovery slightly increases again above 2.75.

As observed from the results for the reduction of EAF slags with high FeO content, the CaO:SiO$_2$ ratio, as a function of iron recovery, requires more stringent control than the initial FeO content to optimize the

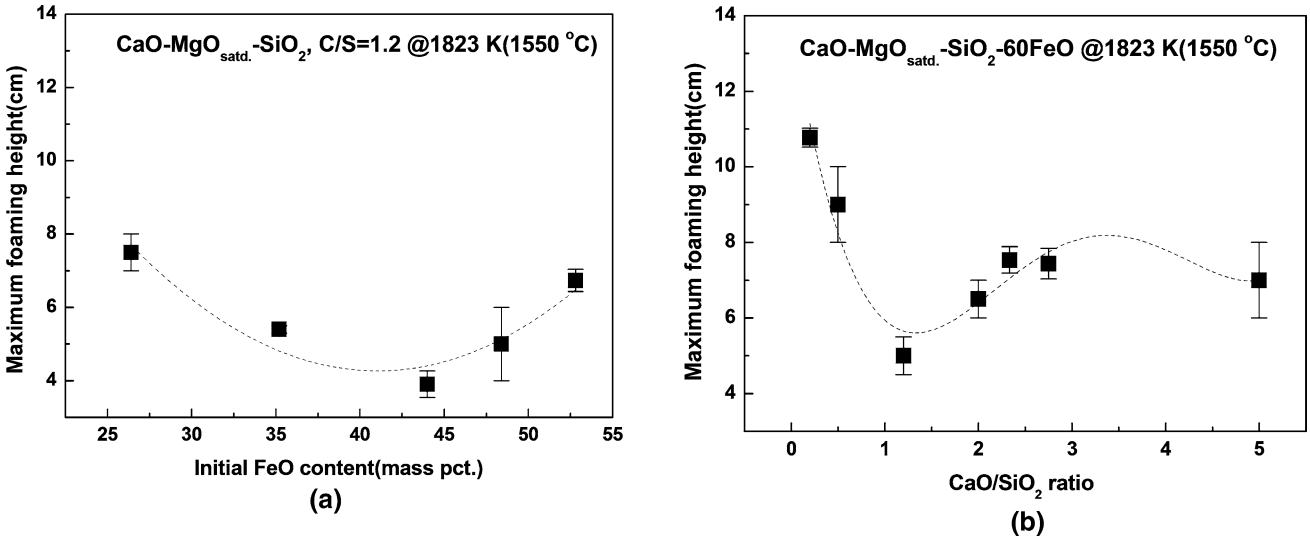

Fig. 5—Effect of varying (*a*) initial FeO content at fixed CaO:SiO$_2$ ratio of 1.2 and (*b*) CaO:SiO$_2$ ratio at FeO 60 mass pct on maximum foaming height in CaO-MgO$_{satd.}$-SiO$_2$-FeO at 1823 K (1550 °C).

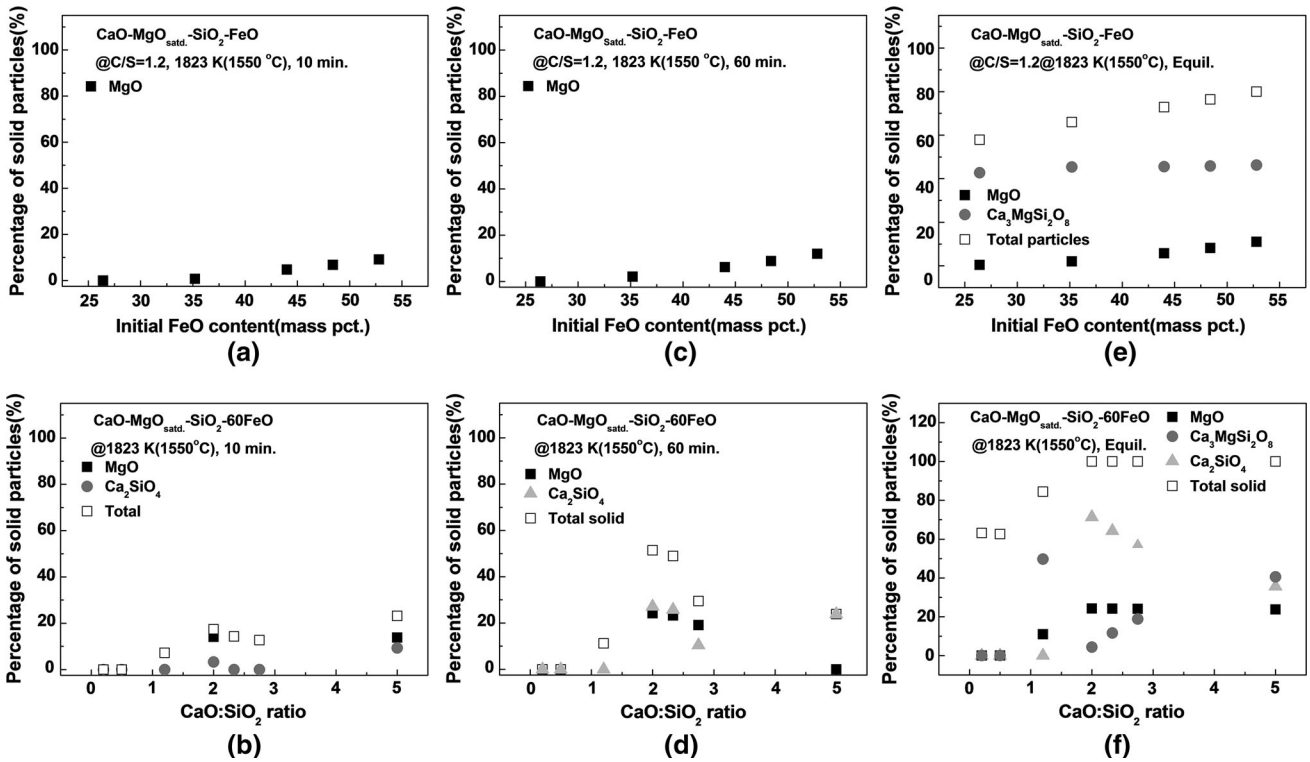

Fig. 6—Solid fraction calculation using FactSage at 1823 K (1550 °C) as a function of varying (*a*) initial FeO content at fixed CaO:SiO$_2$ ratio of 1.2 after 10 min, (*b*) CaO:SiO$_2$ ratio with initial FeO of 60 mass pct after 10 min, (*c*) initial FeO content at fixed CaO:SiO$_2$ ratio of 1.2 after 60 min, (*d*) CaO:SiO$_2$ ratio with initial FeO of 60 mass pct after 60 min, (*e*) initial FeO content at fixed CaO:SiO$_2$ ratio of 1.2 after equilibrium, and (*f*) CaO:SiO$_2$ ratio with initial FeO of 60 mass pct after equilibrium.

iron yield. The presented effect of the initial FeO content and CaO:SiO$_2$ ratio on the iron recovery can be ultimately correlated to the existence of solid particles in the slag and the modified foaming index.

Using the iron recovery and the measured FeO content in the slag after 60 minutes of reduction, the percent of Fe droplets retained in the slag can be ascertained. As expected, the percent of Fe droplets retained in the slag as a function of initial FeO content and CaO:SiO$_2$ ratio is opposite to the trend of iron recovery, and the amount can be significant, as observed in Figure 4. At an optimal initial FeO content of 44 mass pct and higher, approximately 25 to 30 pct of the reduced Fe droplets remain in the slag. At an optimal

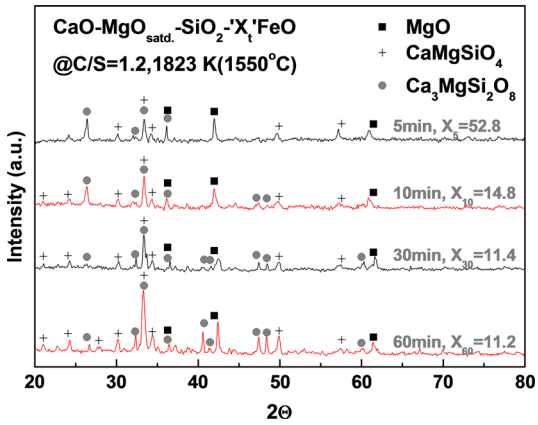

Fig. 7—Characteristic XRD peaks of as-quenched slag samples at various reduction times (5, 10, 30, and 60 min) with fixed CaO:SiO$_2$ ratio of 1.2 at 1823 K (1550 °C). Note the changes in FeO content and the corresponding evolved phases within the slag.

CaO:SiO$_2$ ratio of 1.2, the percent of reduced Fe droplets remaining in the slag is approximately 10 pct. Under certain conditions, unmaximized slags can result in greater than 50 pct Fe droplet retention, which significantly lowers the iron yield of EAF operations.

Figures 5(a) and (b) show the effect of the initial FeO content and the CaO:SiO$_2$ ratio on the maximum foaming height, which can be qualitatively correlated to the modified foaming index. In Figure 5(a), the maximum foaming height as a function of initial FeO content behaves opposite to the iron recovery, where the measured height decreased until reaching an initial FeO content of 44 mass pct, showing a minimum before increasing again with higher initial FeO contents in the slag.

In terms of the maximum foaming height and possible minimization of heat loss through optimal slag foaming practices during EAF operation, the initial FeO content of 44 mass pct may not be a practical option for operation but should be balanced with the iron recovery discussed previously. The maximum foaming height as a function of the CaO:SiO$_2$ ratio also shows a similar trend with a minimum at 1.2 and increasing up to 2.75. At CaO:SiO$_2$ ratios above 2.75, a slight decrease is observed. Accordingly, the minimum foam height was observed at a CaO:SiO$_2$ ratio of 1.2. In addition, with lower foaming, the amount of iron recovery in the iron reservoir seems to increase. However, it should be noted that although excessive foaming is avoided in practice, a moderate amount or tendency for foaming is needed to ensure greater energy efficiency in the EAF.

B. *Evolution of Solid Phases During Reduction*

Solid particles co-existing in the liquid slag can significantly affect the viscosity, which subsequently modifies the foaming index. Thus, it is essential to understand the solidification path as the FeO content is lowered by reduction with carbon. Using FactSage 7.0 and the FToxide database, the solid compound fraction can be thermodynamically estimated according to the FeO content existing in the CaO-MgO$_{satd.}$-SiO$_2$-FeO slag system. In the present work, the thermodynamic calculations were conducted at 1823 K (1550 °C) with an oxygen partial pressure of 10^{-7} atm following the Ellingham diagram, which is in the range confirmed by Barati *et al.*,[31] Heo *et al.*[9] and Lim and Oh[32] for excess carbon injection resulting in reduction and slag foaming.

Figures 6(a) and (b) show the solid particle fraction within the melt after 10 minutes of reduction as a function of initial FeO content at a fixed CaO:SiO$_2$ ratio of 1.2 and as a function of CaO:SiO$_2$ ratio with an initial FeO content of 60 mass pct, respectively. Figures 6(c) and (d) show similar plots for samples taken after 60 minutes of reduction. As FeO is reduced, possible precipitants of MgO and Ca$_2$SiO$_4$ are thermodynamically stable, which is comparable to the results of Heo *et al.*,[9] in the CaO-MgO-SiO$_2$-FeO-Al$_2$O$_3$ slag system, even though MgAl$_2$O$_4$ (spinel) was also observed at the final stages of reduction. Since the starting slag composition is saturated with MgO at the initial FeO content in the slag before carbon addition, the MgO saturation point changes as the reduction proceeds, which affects the solid fraction and foaming behavior of the slag. After 10 minutes, MgO precipitates and increases the fraction of solid particles, which is more pronounced with higher initial FeO contents and CaO:SiO$_2$ ratios. The Ca$_3$MgSi$_2$O$_8$ (merwinite) and Ca$_2$SiO$_4$ solid precipitants are identified predominantly at the final stages shown in Figures 6(e) and (f), with Ca$_2$SiO$_4$ partially formed after 10 minutes only in limited slag compositions of CaO:SiO$_2$ ratios of 2.0 and 5.0.

The solid particle fraction after 10 minutes is larger with higher initial FeO content and CaO:SiO$_2$ ratio, clearly indicating that the oversaturation of MgO is more significant at higher initial FeO contents and CaO:SiO$_2$ ratios. At the equilibrium condition of nearly complete FeO reduction, the available liquid phase is limited and the bulk is solid, as can be observed from the percentage of solid particles with different initial FeO contents and CaO:SiO$_2$ ratios. According to the equilibrium calculations, the majority of the solids are CaO-rich complex oxides.

Figure 7 shows the characteristic XRD peaks of the as-quenched CaO-MgO$_{satd.}$-SiO$_2$-'x_t'FeO slag after reduction for various time intervals. x_t refers to the content of FeO after time 't' (in min). The initial FeO content before reduction was 52.8 mass pct. Complex CaO-MgO-SiO$_2$ intermediate phases are observed, including CaMgSiO$_4$ (monticellite) and Ca$_3$MgSi$_2$O$_8$, along with MgO, even after only 5 minutes of the reduction. From the XRD results of the observed phases and the equilibrium phases predicted from FactSage, it is likely that the reactions in the present work do not reach equilibrium and the solidification path is affected by the kinetics of phase evolution. However, the XRD patterns at 60 minutes indicate a more pronounced characteristic peak for Ca$_3$MgSi$_2$O$_8$ than for CaMgSiO$_4$, suggesting a greater thermodynamic stability, similar to the thermodynamic estimates. Nightingale *et al.*[33] described the phase equilibria of the CaO-SiO$_2$-MgO-FeO slag system using the MTDATA calculation. MgO and Ca$_3$MgSi$_2$O$_8$ were identified near 1773

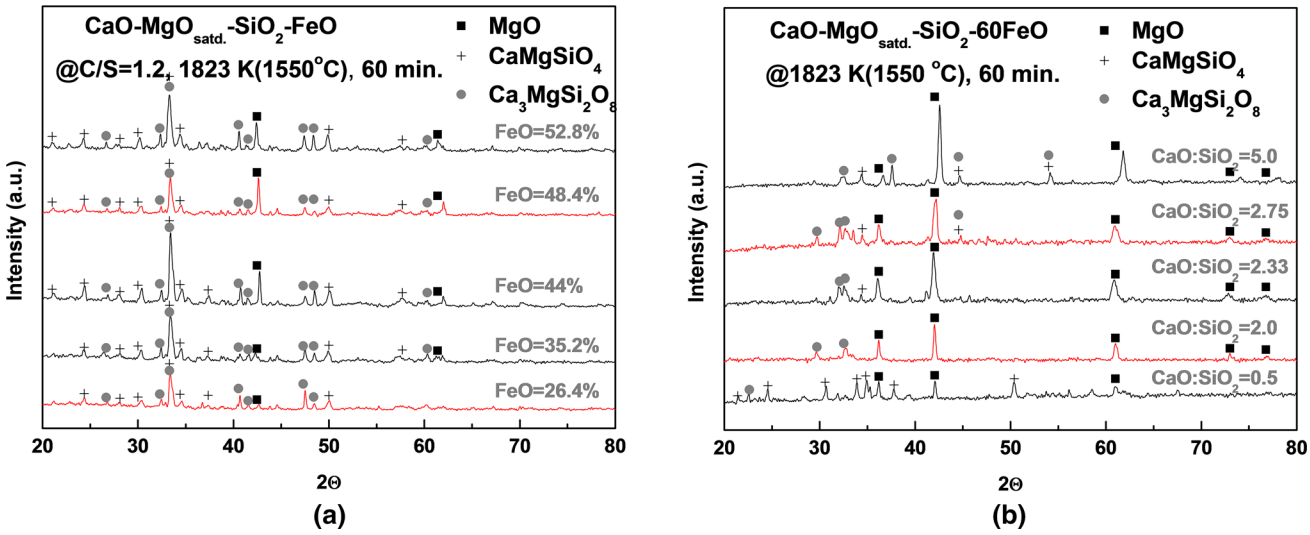

Fig. 8—Characteristic XRD peaks of as-quenched slag samples with varying (*a*) initial FeO content at fixed CaO:SiO_2 ratio of 1.2 and (*b*) CaO:SiO_2 ratio at FeO of 60 mass pct after carbon additions in CaO-$MgO_{satd.}$-SiO_2-FeO at 1823 K (1550 °C) for 60 min.

K (1500 °C) at low FeO mass pct under MgO saturation conditions, and Ca_2SiO_4 was stable at 1750 K (1477 °C) and below. Thus, as the FeO content decreases, the CaO-rich complex phases become more pronounced, which is comparable to the predicted thermodynamic calculations of FactSage in the present study.

Figure 8 shows the XRD patterns after 60 minutes of reduction for various initial FeO contents and CaO:SiO_2 ratios. Although the XRD peaks do not provide a quantitative compositional fraction of the evolved phases, a qualitative comparison can be inferred from the relative peak intensities under identical conditions. MgO was observed and the amount of precipitated CaO-rich complex phases, such as $CaMgSiO_4$ and $Ca_3MgSi_2O_8$, increases with higher initial FeO contents and CaO:SiO_2 ratios near complete reduction. It should be noted that the predicted Ca_2SiO_4 is not observed within 60 minutes of reduction under the conditions in the present study. Although Ca_2SiO_4 is thermodynamically stable, the kinetics are more favorable for the formation of $CaMgSiO_4$ and $Ca_3MgSi_2O_8$ as intermediate phases. This is a topic for further study in the future.

C. *Effect of Solid Compound Precipitation on the Modified Foaming Index from the Surface Tension and Apparent Viscosity*

Figures 9(a) through (d) show the surface tension and apparent viscosities at 1823 K (1550 °C) as a function of initial FeO content at a fixed CaO:SiO_2 ratio of 1.2 and as a function of CaO:SiO_2 ratio at an initial FeO content at 60 mass pct. The apparent viscosity considers the effect of solid compounds co-existing in the liquid melt and is different from the dynamic viscosity.[8,9,18] Both the surface tension and apparent viscosities are essential in estimating the modified foaming index, which directly affect the iron recovery after reduction of FeO in the slag. The surface tension can be estimated using the polynomial function expressed in Eq. [7].[34]

$$\gamma_{l/g} = \sum_{i=1}^{t} X_i \times F_i = X_1F_1 + X_2F_2 + X_3F_3 + X_4F_4 + \cdots + X_tF_t, \quad [7]$$

where $\gamma_{l/g}$ is the surface tension (mN/m), X_i is the mole fraction of component '*i*', and F_i is the surface tension factor of component '*i*' (mN/m). The surface tension factors calculated by Nakamoto *et al.* were used and are provided in Table II.[35,36]

The effect of initial FeO content and CaO:SiO_2 ratio on the surface tension 0 and 10 minutes after carbon insertion is shown in Figures 9(a) and (b), respectively. The surface tension increases with higher initial FeO content and CaO:SiO_2 ratio. The surface tension coefficients of FeO and CaO have higher values than those of the other components comprising the slag. According to previous work, basic oxides such as CaO, MnO, and FeO have higher surface tension coefficients than acidic oxides such as SiO_2.[37] The slope of the surface tension as a function of initial FeO content is less pronounced after carbon reduction for 10 minutes than that of the initial unreduced state. The decrease in FeO, as it is reduced by carbon, plays a major role in minimizing the surface tension. With less FeO in the slag, the amount of available free oxygen anions (O^{2-}) for depolymerizing the structural units of the slag is decreased, and the amount of non-bridged oxygen (O^-) is also decreased.[38,39]

According to Tsarevskii *et al.*[40] and Yuan *et al.*,[41] the addition of CaO increased the surface tension in the CaO-MgO-SiO_2-FeO slag system at 1573 K and 1673 K (1300 °C and 1400 °C) by lowering the interfacial

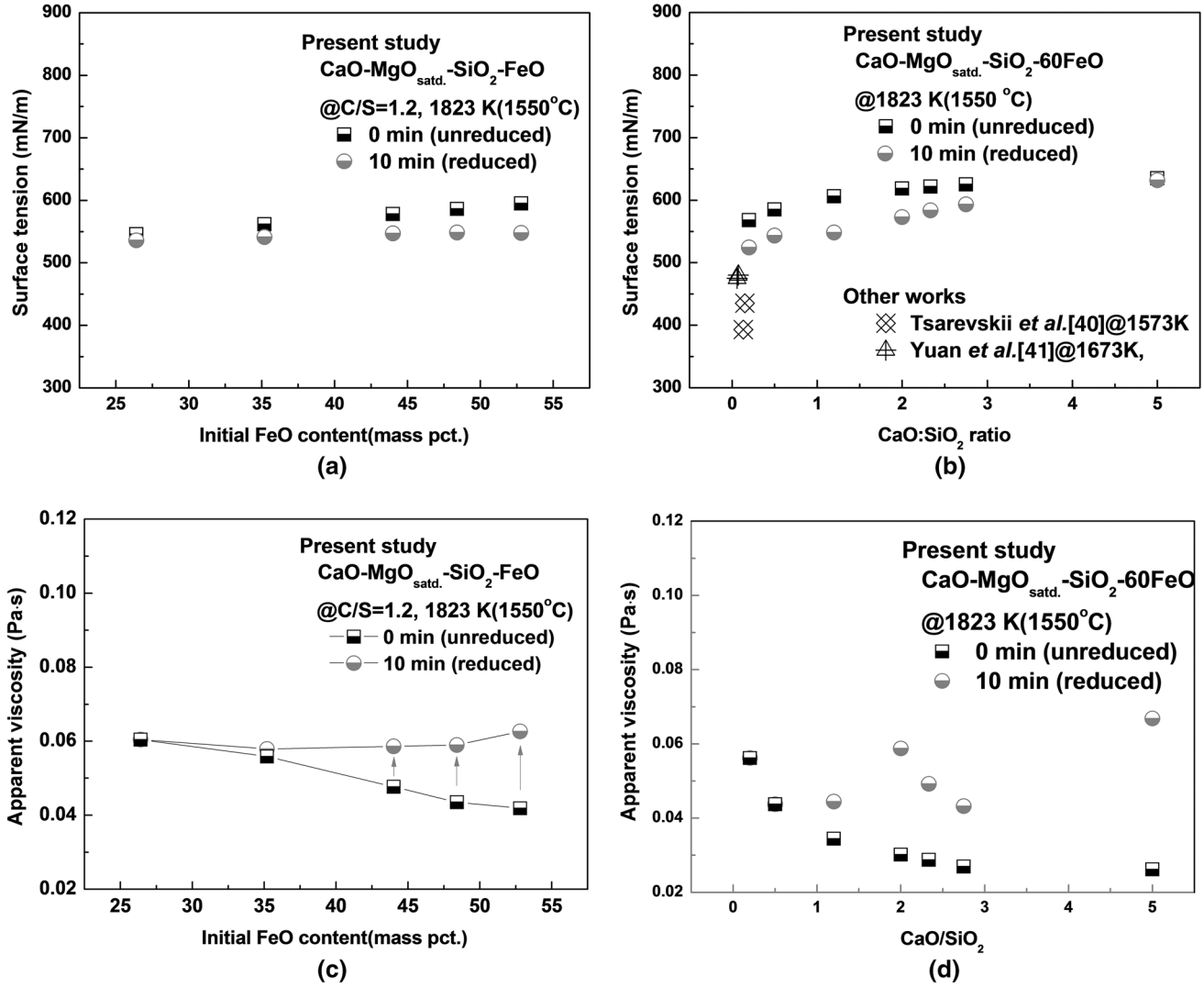

Fig. 9—Calculated surface tension with varying (*a*) initial FeO content at fixed CaO:SiO$_2$ ratio of 1.2 (*b*) CaO:SiO$_2$ ratio at FeO of 60 mass pct and apparent viscosity with varying (*c*) initial FeO content at fixed CaO:SiO$_2$ ratio of 1.2 (*d*) CaO:SiO$_2$ ratio at FeO of 60 mass pct after carbon addition in CaO-MgO$_{satd.}$-SiO$_2$-FeO at 1823 K (1550 °C).

Table II. Surface Tension Factors for the Components in the CaO-MgO$_{satd.}$-SiO$_2$-FeO Slag System Used in the Present Work According to Nakamoto *et al.*[35,36]

	Surface Tension Factor (mN/m)			
	CaO	MgO	SiO$_2$	FeO
σ (T)	791 − 0.0935 × T	1770 − 0.636 × T	243.2 + 0.031 × T	504 + 0.0984 × T
σ (1823 K)	620.54	610.57	299.71	683.38

resistance, which correlates to the higher surface tension observed in the present work with higher CaO/SiO$_2$ ratios, as observed in Figure 9(b).

The viscosity estimated by FactSage as a function of the initial FeO content and as a function of the CaO:SiO$_2$ ratio is provided in Figures 9(c) and (d), respectively. The modified quasi-chemical model was used in the viscosity calculations.[34,42] The viscosity of the unreduced original state decreases with higher initial FeO contents and CaO:SiO$_2$ ratios. Generally, basic oxides of CaO and FeO depolymerize the network structure of the slag formed by acidic oxides such as SiO$_2$ and Al$_2$O$_3$.[43,44] Thus, the supply of free oxygen (O^{2-}) anions from FeO and CaO breaks the bridged oxygen (O°) anions and consequently decreases the viscosity of the slag, as shown in Figures 9(c) and (d).[45,46] After 10 minutes of reduction, significant compositional changes in FeO and the precipitation of solid particles occur, which increases the viscosity.

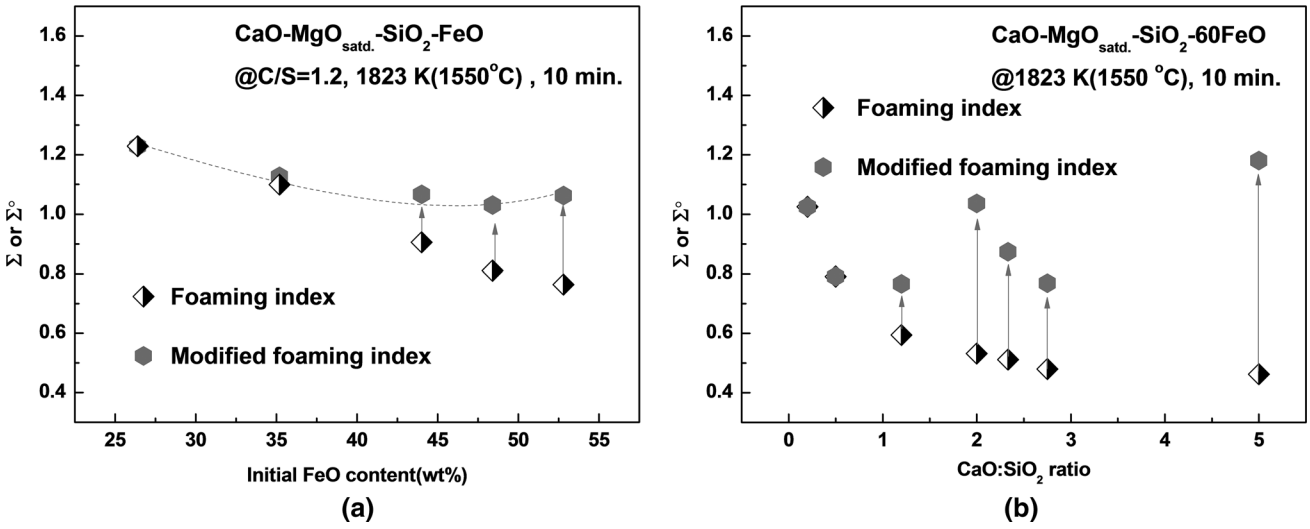

Fig. 10—Effect of varying (*a*) initial FeO content at fixed CaO:SiO$_2$ ratio of 1.2 and (*b*) CaO:SiO$_2$ ratio at FeO of 60 mass pct after carbon additions on foaming indices in CaO-MgO$_{satd.}$-SiO$_2$-FeO at 1823 K (1550 °C).

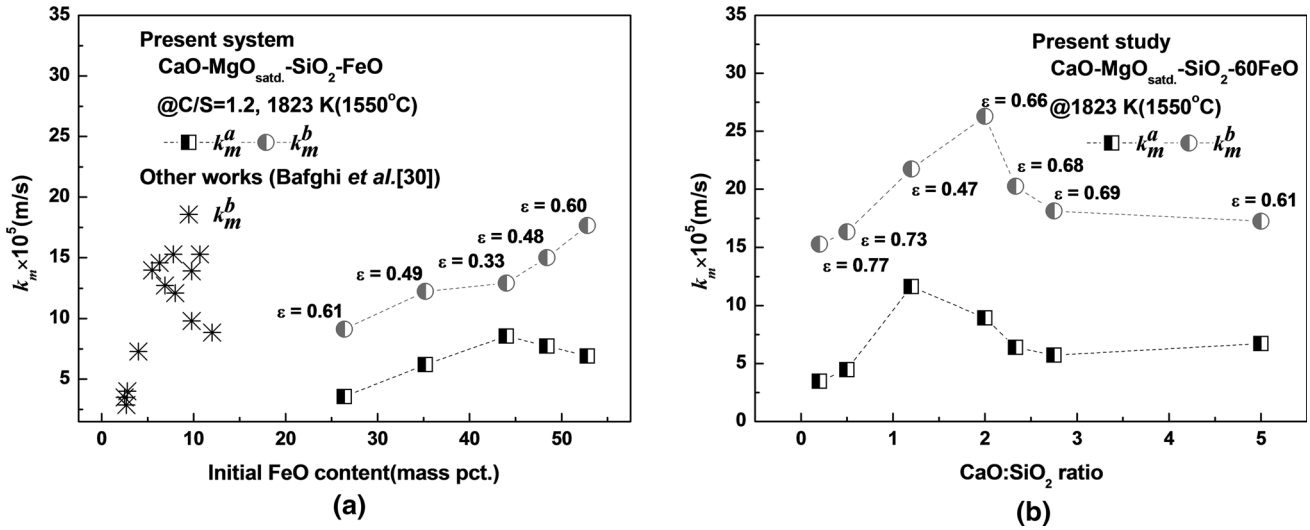

Fig. 11—Effect of varying (*a*) initial FeO content at fixed CaO:SiO$_2$ ratio of 1.2 and (*b*) CaO:SiO$_2$ ratio at initial FeO of 60 mass pct on the mass transfer coefficient (k_m) of FeO in CaO-MgO$_{satd.}$-SiO$_2$-FeO after carbon additions at 1823 K (1550 °C).

The apparent viscosity, which considers the solid particles co-existing in the slag melt and assumes that the solid particles are dispersed uniformly in the liquid slag and exist in spherical form, substantially increases from the initial viscosity. The resulting apparent viscosity can be expressed as Eq. [8] and consequently increases the foaming index.[17,18]

$$\eta = \frac{\eta^{o}}{(1 - \alpha \times f)^{n}}, \qquad [8]$$

where η^{o} and η are the viscosity of the fully liquid slag and the apparent viscosity containing solid fractions, respectively; f is the solid volume fraction in the molten slag; and α and n are empirical constants. The values 1.35 and 2.5 were used for α and n, respectively, in the apparent viscosity calculation.[47] As a result, the apparent viscosity after 10 minutes of reduction, as shown in Figure 9(c), decreases with initial FeO content, showing a minimum between 35.2 and 44 mass pct and increases with higher initial FeO content. Similar effects are observed with the CaO/SiO$_2$ ratio, where the apparent viscosity after 10 minutes of reduction is much higher than that of the unreduced state. As seen in Figure 9(d), a higher CaO:SiO$_2$ ratio initially lowers the apparent viscosity, which agrees with the results of Ji *et al.*[48,49] After 10 minutes of reduction, the apparent viscosity decreases with higher CaO:SiO$_2$ ratios up to 1.2, which agrees with the results of Ji *et al.*[48,49] Above 1.2, the apparent viscosity increases up to a CaO:SiO$_2$ ratio of 2.0 and then follows an upward opening parabola curve.

For the present work, the reduction of FeO by carbon and the initial saturation of MgO in the CaO-MgO$_{satd.}$-SiO$_2$-FeO slag system results in significant

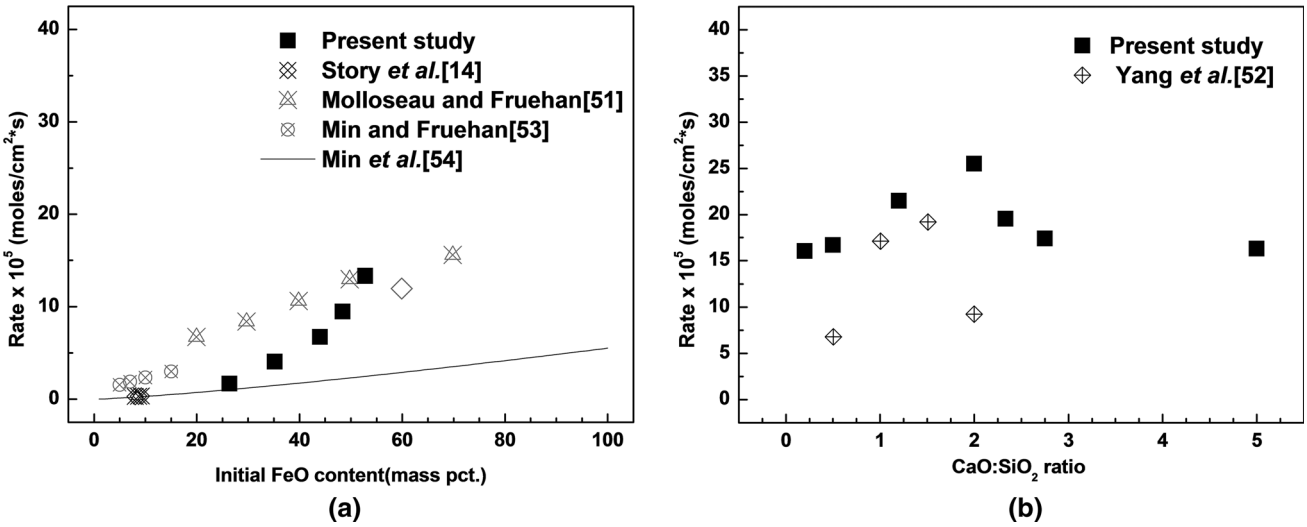

Fig. 12—Effect of varying (*a*) initial FeO content at fixed $CaO:SiO_2$ ratio of 1.2 and (*b*) $CaO:SiO_2$ ratio at fixed FeO of 60 mass pct after carbon additions on the reduction rate per unit area in $CaO\text{-}MgO_{satd.}\text{-}SiO_2\text{-}FeO$ at 1823 K (1550 °C).

compositional changes in the slag and the phases present. The apparent viscosity after 10 minutes of reduction is significantly changed compared to its initial viscosity due to the variation in slag composition and precipitation of solid compounds such MgO and $Ca_3Mg(SiO_4)_2$, as revealed by XRD and FactSage, as previously illustrated. Using the apparent viscosity in Eq. [6], an empirical correlation for slag foaming that considered the co-existence of secondary solid compounds within the slag melt was developed.

Figures 10(a) and (b) show the calculated foaming index and the modified foaming index as a function of the initial FeO content and $CaO:SiO_2$ ratio using the surface tension and apparent viscosities provided in Figures 9(a) through (d). The effect of the solid fraction on the foaming index becomes significant above an initial FeO content of 40 mass pct and above a $CaO:SiO_2$ ratio of 1.2. Thus, the behavior of iron recovery after reduction with carbon can ultimately be correlated to the presence of solid phases co-existing within the liquid slag and the subsequently modified foaming index. Therefore, within the experimental conditions of the present work, the iron recovery after reduction as a function of varying initial FeO content and $CaO:SiO_2$ ratio is significantly inhibited by a higher modified foaming index, and thus, the iron recovery and modified foaming index show opposite trends.

D. *Kinetics of FeO Reduction in Slag with Carbon Flakes*

In the present slag system, rapid reduction occurs within 10 minutes, which was verified by measuring the FeO concentration over time. Assuming the liquid-phase mass transfer of FeO in the slag is rate limiting, the reaction at the FeO and carbon interface is fast and reaches equilibrium. Equation [9] can be used to derive the relationship between the FeO content at time '*t*' (mass pct FeO^t) and the initial time '*i*' (mass pct FeO^i).

$$-\ln\left(\frac{\text{mass pct FeO}^t}{\text{mass pct FeO}^i}\right) = \left(\frac{k_m \times A}{V_o}\right) \times t, \qquad [9]$$

where A (m^2) and k_m (m/s) are the reaction area and the mass transfer coefficient, respectively, and V_o (m^3) is the slag volume neglecting slag foaming. The reaction area was calculated from the total surface area of the carbon flake assuming the rectangular parallelepiped dimensions previously provided. To obtain the FeO mass transfer coefficient, the concentration of FeO as a function of time was linearly fitted within the active 10 minutes reduction region of the present study. The slag volume and the density were obtained using appropriate literature values that corresponded to the conditions of the present experiment.[19,20]

The FeO mass transfer coefficient as a function of the initial FeO content and $CaO:SiO_2$ ratio is shown in Figures 11(a) and (b), respectively. The mass transfer coefficient neglecting slag foaming (k_m^a) increased with higher initial FeO content up to 44 mass pct and decreased with further addition. The mass transfer coefficient also increases with higher $CaO:SiO_2$ ratio up to 1.2 and decreases until 2.75. Between 2.75 and 5.0, the mass transfer coefficient slightly increases. However, foaming is significant during the reduction of FeO, and k_m^a does not correctly reflect the present system with slag foaming.

Previous works have described the effect of generated gases, such as CO and CO_2, on the FeO mass transfer coefficient in the slag, where large volumes of gases generated could agitate the slag and promote foaming. Using the gas holdup factor (ε), the effect of the gas on the mass transfer coefficient can be mathematically evaluated, as provided previously.[10,50] The gas holdup factor is the ratio of the volume of the foamed slag minus the unfoamed original slag volume over the total volume of the foamed slag. Using the gas holdup factor, the mass transfer coefficient considering slag foaming (k_m^b) can be expressed as Eq. [10].

$$k_m^b = \frac{k_m^a}{1-\varepsilon} \quad [10]$$

Notably, k_m^b increases with higher initial FeO content, and the increment of the slope is significantly higher above 44 mass pct, as shown in Figure 11(a). This result seems to correlate with increased solid compound formation, as provided in Figure 6(a). As expected, the mass transfer coefficient increases with greater foaming in the slag. A similar behavior was observed with the $CaO:SiO_2$ ratio, as illustrated in Figure 11(b). Bafghi *et al.*[10,13] also calculated k_m^b at low initial FeO ranges at 1573 K (1300 °C) and also showed the mass transfer coefficient to increase with higher initial FeO content within the range of 5 to 10 mass pct due to slag foaming. Even though Bafghi *et al.*[10,13] worked at lower FeO ranges, their mass transfer coefficient is slightly higher than that in the present study due to the difference in experimental temperature and subsequent increased solid compound formation, which induced slag foaming.

To validate the estimated mass transfer coefficient (k_m^b) of the present slag system with previously published works, the reduction rate correlated to the flux of FeO using k_m^b was calculated with the units of moles/cm^2 s, as depicted in Figures 12(a) and (b).[51] Similar reduction rates can be observed in previous works, and the rate increased with higher initial FeO, as shown in Figure 12(a). Slight discrepancies in the calculated fluxes seem to be caused by the compositional and temperature differences in the experimental conditions. Similar trends can be observed in Figure 12(b) with respect to the $CaO:SiO_2$ ratio. Yang *et al.*[52] indicated that the rate constant is highest near a $CaO:SiO_2$ ratio of 1.5 in the $CaO\text{-}SiO_2\text{-}Fe_tO\text{-}Al_2O_3$ slag system, which was also observed in the present study within the $CaO:SiO_2$ ratio range of 1.2 to 2.0.

Under the conditions in the present work, the mass transfer coefficient is improved with greater slag foaming. However, although the FeO mass transfer coefficient is increased and the subsequent reduction is promoted by the apparent agitation, iron recovery shows the opposite trend to that of the reduction kinetics because excessive gas evolution prevents the reduced Fe droplets from collecting in the molten iron reservoir. At a $CaO:SiO_2$ ratio of 2.0, the mass transfer coefficient is maximized, but the maximum iron recovery occurred at a $CaO:SiO_2$ ratio of 1.2. Thus, greater mass transport and subsequent faster reduction do not necessarily result in optimal iron recovery. This is also evident in the iron recovery depending on the initial FeO content, where the recovery ratio was greatest at 44 mass pct but the mass transfer coefficient was highest above 44 mass pct. Accordingly, gas evolution accelerated mass transport of the reactants to the reaction sites and subsequently enhanced the reduction, but the collection of Fe droplets in the molten iron reservoir was significantly impaired. Thus, determination of the optimal compositional range and foaming behavior considering solid compound precipitants is necessary for these reasons.

IV. CONCLUSION

The effect of the initial FeO content and $CaO:SiO_2$ ratio on the behavior of FeO reduction was identified in the $CaO\text{-}MgO_{satd.}\text{-}SiO_2\text{-}FeO$ EAF slag system. The following main results were identified from this study.

1. The modified foaming index was calculated considering the solid compound fraction forming during the reduction of FeO in an initially MgO-saturated quaternary slag system. The trend of the modified foaming index with respect to the initial FeO content in the slag and the $CaO:SiO_2$ ratio behaved opposite to that of iron recovery, where the greater foaming ability of the slag inhibited recovery of the reduced Fe droplets. The behavior of the maximum foaming height was experimentally measured and qualitatively correlated to the estimated foaming index.
2. Due to the apparent viscosity, solid compound precipitation during reduction, and the subsequent effect on the modified foaming index, iron recovery was maximized at a $CaO:SiO_2$ ratio of 1.2 and an initial FeO content of approximately 44 mass pct and above. However, a balance between slag foaming for increased energy efficiency in the EAF and iron recovery for greater yield should also be considered during EAF operation.
3. The solid compound fraction was identified by XRD and FactSage. The thermodynamic equilibrium phases estimated through FactSage did not coincide with the as-quenched samples confirmed by XRD. Intermediate phases of CaO-rich complex oxides were evident in the samples, suggesting that the phase evolution kinetics also play a significant role in the solid fractions formed during the reduction smelting process.
4. Slag foaming by gases generated from FeO reduction was considered in the determination of the FeO mass transfer coefficient. The modified mass transfer coefficient considering slag foaming was calculated using the gas holdup factor, but the value did not coincide with the observed iron recovery. Thus, the reduction kinetics are accelerated by slag foaming, but the final iron collection in the iron reservoir was inhibited with excessive gas evolution and foaming.

ACKNOWLEDGMENTS

This study was supported by the Brain Korea 21 (BK21) Project of the Division of Humantronics Information Materials Grant No. 2016-11-0010 and the Ministry of Trade, Industry and Energy Grant No. 10044705.

REFERENCES

1. T. Zhu: *Carbon Injection into Electric Arc Furnace Slags*, Doctoral dissertation, McMaster University, 2012, pp. 1–94.
2. B. Lee and I. Sohn: *JOM*, 2014, vol. 66, pp. 1581–94.

3. J.A. de Araújo and V. Schalch: *J. Mater. Res. Technol.*, 2014, vol. 3, pp. 274–79.
4. B. Lee, J.W Ryu, and I. Sohn: *Steel Res. Int.*, 2015, vol. 86, pp. 302–09.
5. M. Ozawa, S. Kitagawa, S. Nakayama, and Y. Takesono: *Trans. ISIJ*, 1986, vol. 26, pp. 621–28.
6. J. Dankwah, P. Koshy, and V. Sahajwalla: *Ironmak. Steelmak.*, 2014, vol. 41, pp. 401–09.
7. G. Qiu, C. Shan, X. Zhang, and X. Lv: *Ironmak. Steelmak.*, 2017, vol. 44, pp. 246–54.
8. D. Busolic, F. Parada, R. Parra, M. Sanchez, J. Palacios, and M. Hino: *Min. Process. Extract. Metall.*, 2011, vol. 120, pp. 32–36.
9. J.H. Heo, B.S. Kim, and J.H. Park: *Metall. Mater. Trans. B*, 2013, vol. 44, pp. 1352–63.
10. M.S. Bafghi, H. Kurimoto, and M. Sano: *ISIJ Int.*, 1992, vol. 32, pp. 1084–90.
11. R.K. Paramguru, R.K. Galgali, and H.S. Ray: *Metall. Mater. Trans. B*, 1997, vol. 28, pp. 805–10.
12. M.W. Davies, P.N. Smith, and G.S.F. Hazeldean: *Proceedings The Richardson Conference*, H.E. Jeffes, ed., BSC, Sheffield, United Kingdom, 1973, pp. 95–107.
13. M.S. Bafghi, Y. Ito, S. Yamada, and M. Sano: *ISIJ Int.*, 1992, vol. 32, pp. 1280–86.
14. S. Story, B. Sarma, R. Fruehan, A. Cramb, and G. Belton: *Metall. Mater. Trans. B*, 1998, vol. 29, pp. 929–32.
15. M. Zaharia, V. Sahajwalla, R. Khanna, and P. Koshy: *ISIJ Int.*, 2009, vol. 49, pp. 1513–21.
16. R. Corbari, H. Matsuura, S. Halder, M. Walker, and R.J. Fruehan: *Metall. Mater. Trans. B*, 2009, vol. 40, pp. 940–48.
17. K. Ito and R. Fruehan: *Metall. Mater. Trans. B*, 1989, vol. 20, pp. 509–14.
18. K. Ito and R. Fruehan: *Metall. Mater. Trans. B*, 1989, vol. 20, pp. 515–21.
19. B.J. Keene and K.C. Mills: *Slag Atlas*, 2nd ed., Verein Deutscher Eisenhüttenleute, eds., Verlag Stahleisen, Düsseldorf, 1995, pp. 313–48.
20. K.C. Mills and B.J. Keene: *Int. Mater. Rev.*, 2013, vol. 32 (1), pp. 1–120.
21. R. Jiang and R. Fruehan: *Metall. Mater. Trans. B*, 1991, vol. 22, pp. 481–89.
22. H.S. Kim, D.J. Min, and J.H. Park: *ISIJ Int.*, 2001, vol. 41, pp. 317–24.
23. S. Mostafaee: *A Study of EAF High-Chromium Stainless Steelmaking Slags Characteristics and Foamability*, Doctoral dissertation, KTH Royal Institute of Technology, 2011.
24. K.C. Mills, L. Yuan, and R. Jones: *J. SAIMM*, 2011, vol. 111, pp. 649–58.
25. R.D. Morales, L.G. Rubén, F. López, J. Camacho, and J.A. Romero: *ISIJ Int.*, 1995, vol. 35, pp. 1054–62.
26. H. Suito and R. Inoue: *Trans. ISIJ*, 1984, vol. 24, pp. 301–07.
27. H. Suito, R. Inoue, and M. Takada: *Trans. ISIJ*, 1981, vol. 21, pp. 250–59.
28. J.Y. Park, S.M. Jung, and I. Sohn: *Metall. Mater. Trans. B*, 2014, vol. 45, pp. 329–33.
29. S.S. Jung and I. Sohn: *Environ. Sci. Technol.*, 2014, vol. 48, pp. 1886–92.
30. M.S. Bafghi, M. Fukuda, Y. Ito, S. Yamada, and M. Sano: *ISIJ Int.*, 1993, vol. 33, pp. 1125–30.
31. M. Barati and K.S. Coley: *Metall. Mater. Trans. B*, 2005, vol. 36, pp. 169–78.
32. S. Lim and M. Oh: *Korean J. Chem. Eng.*, 2007, vol. 24, pp. 911–16.
33. S.A. Nightingale, B.J. Monaghan, and G.A. Brooks: *Metall. Mater. Trans. B*, 2005, vol. 36, pp. 453–61.
34. C. Bale, E. Bélisle, P. Chartrand, S. Decterov, G. Eriksson, K. Hack, I.-H. Jung, Y.B. Kang, J. Melançon, and A. Pelton: *Calphad*, 2009, vol. 33, pp. 295–311.
35. M. Nakamoto, M. Hanao, T. Tanaka, M. Kawamoto, L. Holappa, and M. Hämäläinen: *ISIJ Int.*, 2007, vol. 47, pp. 1075–81.
36. M. Nakamoto, A. Kiyose, T. Tanaka, L. Holappa, and M. Hämäläinen: *ISIJ Int.*, 2007, vol. 47, pp. 38–43.
37. J.B. Kim, J.K. Choi, I.W. Han, and I. Sohn: *J. NonCryst. Solids*, 2016, vol. 432, pp. 218–26.
38. J.B. Kim and I. Sohn: *ISIJ Int.*, 2014, vol. 54, pp. 2050–58.
39. E.J. Jung and D.J. Min: *Steel Res. Int.*, 2012, vol. 83, pp. 705–11.
40. B. Tsarevskii, S. Popel, and V. Eremenko: *The Role of Surface Phenomena in Metallurgy*, Consultants Bureau, New York, 1963, p. 96.
41. Z. Yuan, M. Sun, and X. Chen: *Youse Jinshu-Nonferrous Metals China*, 1988, vol. 40, pp. 58–64.
42. A. Kondratiev, P.C. Hayes, and E. Jak: *ISIJ Int.*, 2006, vol. 46, pp. 359–67.
43. M. Kucharski, N.M. Stubina, and J.M. Toguri: *Can. Metall. Quart.*, 2013, vol. 28, pp. 7–11.
44. Y.S. Lee, D.J. Min, S.M. Jung, and S.H. Yi: *ISIJ Int.*, 2004, vol. 44, pp. 1283–90.
45. L. Bodnar, K. Tomasek, L. Bobok, and J. Schmiedl: *Hutn. Listy.*, 1978, vol. 33, pp. 497–501.
46. P. Williams, M. Sunderland, and G. Briggs: *T. I. Min. Metall. C*, 1983, vol. 92, pp. 105–09.
47. S.H. Seok, S.M. Jung, Y.S. Lee, and D.J. Min: *ISIJ Int.*, 2007, vol. 47, pp. 1090–96.
48. F.Z. Ji: *Metall. Mater. Trans. B*, 2001, vol. 32, pp. 181–86.
49. F.Z. Ji, D. Sichen, and S. Seetharaman: *Metall. Mater. Trans. B*, 1997, vol. 28, pp. 827–34.
50. L. Hong, M. Hirasawa, and M. Sano: *ISIJ Int.*, 1998, vol. 38, pp. 1339–45.
51. C. Molloseau and R. Fruehan: *Metall. Mater. Trans. B*, 2002, vol. 33, pp. 335–44.
52. Z. Yang, M. Rui-lin, N. Wang-dong, and W. Hui: *Hydrometallurgy*, 2010, vol. 103, pp. 25–29.
53. D.J. Min and R.J. Fruehan: *Metall. Mater. Trans. B*, 1992, vol. 23, pp. 29–37.
54. D.J. Min, J.W. Han, and W.S. Chung: *Metall. Mater. Trans. B*, 1999, vol. 30, pp. 215–21.